

Low-Temperature Processed and Carbon-Based ZnO/CH₃NH₃PbI₃/C Planar Heterojunction Perovskite Solar Cells

Huawei Zhou,[†] Yantao Shi,^{*,†} Kai Wang,[†] Qingshun Dong,[†] Xiaogong Bai,[†] Yujin Xing,[†] Yi Du,[†] and Tingli Ma^{*,†,§}

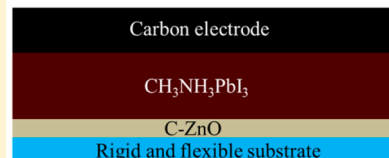
[†]State Key Laboratory of Fine Chemicals, School of Chemistry, Dalian University of Technology, Dalian 116024, China

[§]Graduate School of Life Science and Systems Engineering, Kyushu Institute of Technology, 2-4 Hibikino, Wakamatsu, Kitakyushu, Fukuoka 808-0196, Japan

Supporting Information

ABSTRACT: Carbon-based ZnO/CH₃NH₃PbI₃/C planar heterojunction perovskite solar cells (PHJ-PSCs) were prepared at low-temperature without using organic hole conductor and metal electrode. When measured via reverse bias scan, rigid and flexible PHJ-PSCs achieved power conversion efficiencies (PCEs) up to 8% and 4% on fluorine-doped tin oxide (FTO)/glass substrates and flexible polymer substrates, respectively. The flexible devices were capable of maintaining 80% of their initial PCEs after 1000 times of bending.

Low-temperature Processed and Carbon-based ZnO/CH₃NH₃PbI₃/C Planar Heterojunction Perovskite Solar Cells



1. INTRODUCTION

Organometal trihalide perovskites have attracted attention as new visible-light sensitizers for liquid-state dye-sensitized solar cells¹ or quantum-dot-sensitized solar cell.^{1,2} In the last two years, high power conversion efficiencies (PCEs) up to 15% have been achieved by mesoscopic solar cells based on solid-state p-type hole transport materials (HTMs).^{3,4} Snaith et al. reported that these meso-superstructures^{5–8} and planar heterojunction perovskite solar cells (PSCs) obtain high PCEs.⁹ Yang et al. reported a remarkably high PCE of 19.3% from planar PSCs by interface engineering.¹⁰ PSCs have demonstrated impressive PCEs; however, the unsatisfying durability and costly price of HTMs and metal electrodes (Au and Ag) limit their future large-scale application.

Recently, mesoscopic PSCs that use carbon as an electrode have emerged as a promising low-cost photovoltaic device with better stability.^{11–13} In addition to mesoporous TiO₂, such PSCs still contain ZrO₂ as space layer and require high sintering temperature at ca. 500 °C, which in turn increases the energy pay-back time and limits their mass production and fabrication on polymer flexible substrate. Several attempts have been made to develop flexible PSCs. However, these devices still require HTM and metal electrode that must be prepared through high-vacuum evaporation.^{14–20}

In this present work, we employed carbon as an electrode to prepare hole-conductor-free, metal-electrode-free planar heterojunction perovskite solar cells (PHJ-PSCs) at low temperature on rigid and flexible substrates. Compared with previous reports, our novel carbon-based devices ZnO/CH₃NH₃PbI₃/C are much more simple in their architecture, in which the CH₃NH₃PbI₃ thin film was sandwiched between ZnO (as the electron-selective layer) and carbon electrode (as the hole-selective layer). Under AM 1.5 G and 100 mW cm⁻² simulated

sunlight illumination, the rigid and flexible low-temperature processed PHJ-PSCs achieved PCEs up to 8.73% and 4.29%, respectively. In particular, the flexible devices could maintain 80% of their initial PCEs after 1000 times of bending.

2. EXPERIMENTAL SECTION

Synthesis of ZnO Nanoparticles. ZnO nanoparticles were synthesized using an adapted procedure based on previous work.¹⁴ Zinc acetate dihydrate (11.8 g) was dissolved in methanol (500 mL) with vigorous stirring at 65 °C. Subsequently, a solution of KOH (Tianjin Dalu, 82%, 5.92 g) in methanol (260 mL) was added dropwise at 65 °C over a period of 30 min. Precipitation of zinc hydroxides was formed after 15 min, but dissolved again. After 80 min, the solution became translucent and remained translucent. The reaction mixture was stirred for 2.5 h at 65 °C. Precipitate and supernatant were separated, and the precipitate was washed twice with methanol (80 mL). n-Butanol (200 mL), methanol (14 mL) and chloroform (14 mL) were added to disperse the precipitate and produce a ZnO nanoparticle stock solution with a concentration of 8 mg mL⁻¹. The ZnO nanoparticle solution was filtered through a polyvinyl difluoride (PVDF) syringe filter with a 0.45 μm pore size before use.

Preparation of Low Temperature Conductive-Carbon Paste.²¹ First, low-cost commercial conductive-carbon paste was dried at 120 °C for 1 h to remove the solvent, which can destroy the structure of perovskite. Subsequently, the dried conductive-carbon sample (5 g) and zirconium dioxide pearl (4 g) were dispersed in chlorobenzene (15 mL) and milled for 2 h

Received: December 4, 2014

Revised: February 13, 2015

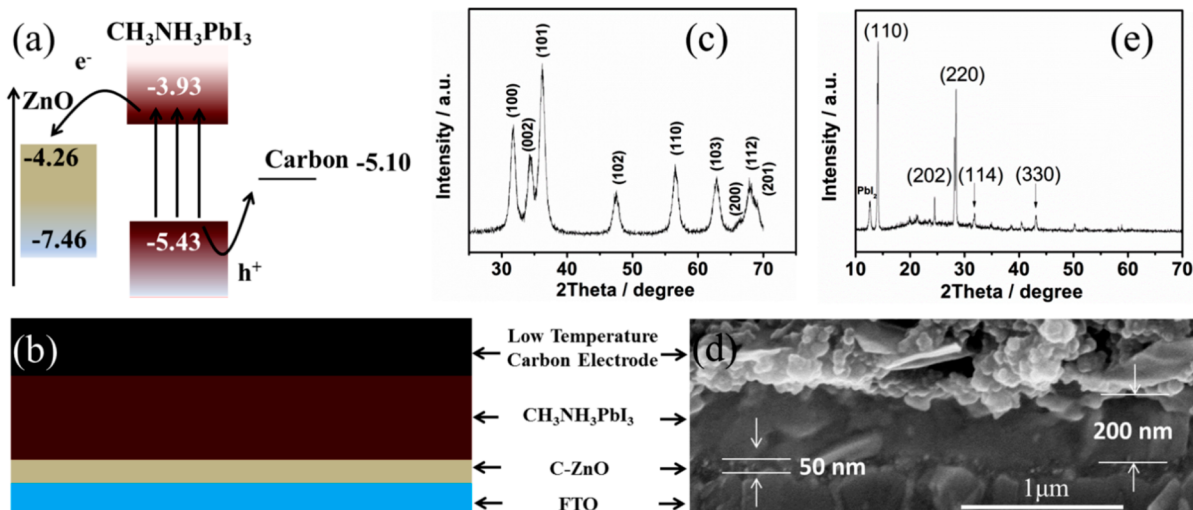


Figure 1. (a) Energy-level diagram of ZnO, $\text{CH}_3\text{NH}_3\text{PbI}_3$, and carbon. (b) Schematic diagram of the architectures of the PHJ-PSCs. (c) XRD spectra of ZnO powder of compact layer. (d) Cross-sectional amplified SEM image of ZnO/ $\text{CH}_3\text{NH}_3\text{PbI}_3$ /C PHJ-PSCs. (e) XRD spectra of the ZnO/ $\text{CH}_3\text{NH}_3\text{PbI}_3$ films prepared on glass.

in an electro-mill (QM-QX0.4, Instrument Factory of Nanjing University).

Device Fabrication of All Low-Temperature Processed ZnO/ $\text{CH}_3\text{NH}_3\text{PbI}_3$ /C PHJ Solar Cells on Rigid Fluorine-Doped Tin Oxide (FTO)/Glass or Flexible Indium Tin Oxide (ITO)/Polyethylene Naphthalate (PEN). First, a thin ZnO nanoparticle layer was prepared by spin coating onto the etched substrate, followed by drying at 120 °C for 1 h. A $\text{CH}_3\text{NH}_3\text{PbI}_3$ thin layer was prepared according to a two-step sequential deposition method.¹⁴ A PbI₂ solution (dissolved in *N,N*-dimethylformamide at a concentration of 462 mg mL⁻¹) was deposited by spin coating on top of the ZnO layer at 3000 r.p.m. for 15 s. After drying for 30 min in a glovebox at room temperature, the substrate was dipped into a solution of $\text{CH}_3\text{NH}_3\text{I}$ in 2-propanol (10 mg mL⁻¹) for 40 s, then dried in a glovebox for 1 h at room temperature. Finally, the carbon electrodes were prepared by doctor-blade coating conductive-carbon paste on the $\text{CH}_3\text{NH}_3\text{PbI}_3$ layer, using pieces of adhesive tape as the pattern and spaces, followed by drying at room temperature for 1 h. The device fabrication was carried out under controlled atmospheric conditions and a humidity of around 1% in the glovebox.

Measurement and Characterization. X-ray diffraction (XRD) patterns were obtained using a PANalytical X'Pert diffractometer ($\text{Cu K}\alpha$ radiation at $\lambda = 1.54 \text{ \AA}$) sampling at 10°/min, 40 kV, and 100 mA. Nanostructures of our samples were characterized and analyzed by scanning electron microscopy (SEM, Nova Nano SEM 450). The photocurrent–voltage performance of the ZnO/ $\text{CH}_3\text{NH}_3\text{PbI}_3$ /C was measured with a metal mask with an aperture area of 0.12 cm² by a Keithley digital source meter (Keithley 2601, USA) equipped with a solar simulator (PEC-L15, Peccell, Yokohama, Japan). The Mott–Schottky plot were measured in the dark with a computer-controlled electrochemical workstation (Zennium Zahner, Germany). The frequency was 1 kHz at bias potentials between 0.2 and 1.4 V.

3. RESULTS AND DISCUSSION

Figure 1a demonstrates the energy level diagram of ZnO, $\text{CH}_3\text{NH}_3\text{PbI}_3$, and carbon. The electrons and holes originated from ambipolar perovskite and should be capable to inject

efficiently into *n*-type ZnO and carbon electrode, respectively. Figure 1b shows the designed architecture of ZnO/ $\text{CH}_3\text{NH}_3\text{PbI}_3$ /C PHJ-PSCs in this study. ZnO compact layer was prepared by spin-coating ZnO nanoparticle solution (8 mg/mL) onto FTO/glass or ITO/PEN and dried at 120 °C for 1 h. The XRD pattern of ZnO powder (Figure 1c) can be assigned to hexagonal ZnO, approximately 11.8 nm in crystal diameter, after being analyzed by the Scherrer equation.²² The diffraction peaks of 31.86°, 34.26°, 36.22°, 47.57°, 56.41°, 62.85°, 66.25°, 68.03°, and 69.39° were attributed to the planes of (100), (002), (101), (102), (110), (103), (200), (112), and (201) for ZnO (36-1451, PDF 2 database), respectively. $\text{CH}_3\text{NH}_3\text{PbI}_3$ was prepared via the two-step sequential deposition method at room temperature according to a literature.¹² Subsequently, carbon electrodes were prepared by doctor-blade coating of conductive-carbon paste on top of the $\text{CH}_3\text{NH}_3\text{PbI}_3$ layer and dried at room temperature for 1 h in a glovebox.²¹ Figure 1d shows a cross-sectional amplified SEM image of low-temperature processed ZnO/ $\text{CH}_3\text{NH}_3\text{PbI}_3$ /C PHJ-PSCs on FTO/glass. The $\text{CH}_3\text{NH}_3\text{PbI}_3$ layer was approximately 200 nm in thickness, and the as-formed $\text{CH}_3\text{NH}_3\text{PbI}_3$ film had good surface coverage on the underlying *n*-type semiconductor ZnO. The crystalline $\text{CH}_3\text{NH}_3\text{PbI}_3$ reached microscale. In the XRD pattern of $\text{CH}_3\text{NH}_3\text{PbI}_3$ on ZnO (Figure 1e), the main diffraction peaks at 14.18°, 24.43°, 28.38°, 31.78° and 43.21° could be assigned to the (110), (202), (220), (114) and (330) peaks, respectively, indicating an orthorhombic crystal structure.^{9,23} The diffraction peaks at 12.63° were attributed to the PbI₂.

To study the effect of electron-selective layer thickness on device performance, we prepared a ZnO electron-selective layer by different spin-coating conditions. The electron-transport layer in Figure 2a,b,c,d are 25, 36, 55, and 89 nm in mean thickness, respectively. Figure 3 shows the device performance for ZnO/ $\text{CH}_3\text{NH}_3\text{PbI}_3$ /C PHJ-PSCs prepared with varying thicknesses of ZnO. The detailed photovoltaic parameters are summarized in Table 1. Electron-selective layer was very important to obtain high-performance devices. From the cross-sectional SEM image in Figure 2a, the very thin ZnO layer was not completely covered on the rough FTO surface. Corresponding top-view SEM images (Figure 2e) further

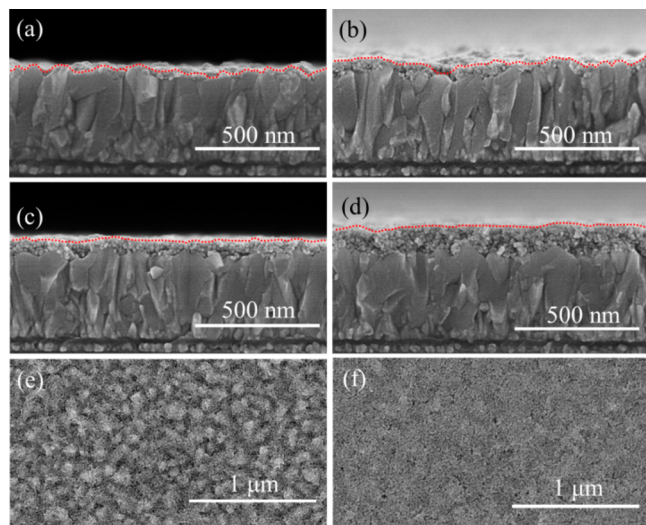


Figure 2. Cross-sectional and top-view SEM images of different spin-coating condition for ZnO compact layer: (a,e) 3000 rpm/min, 30 s, one layer; (b) 1000 rpm/min, 30 s, one layer; (c,f) 1000 rpm/min, 30 s, two layers; (d) 1000 rpm/min, 30 s, three layers.

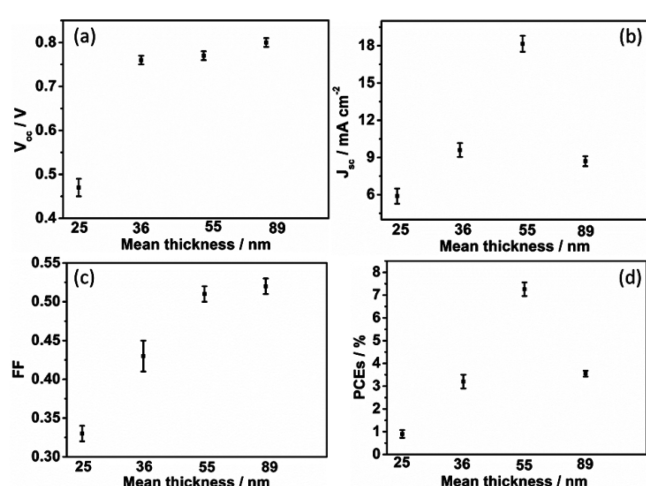


Figure 3. Device parameters for ZnO/CH₃NH₃PbI₃/C PHJ-PSCs prepared with varying thicknesses of ZnO.

Table 1. Device Parameters for ZnO/CH₃NH₃PbI₃/C PHJ-PSCs Prepared with Varying Thicknesses of ZnO

mean thickness/ nm	V _{oc} /V	J _{sc} /mA cm ⁻²	FF	PCE/%
25	0.47 ± 0.02	5.89 ± 0.61	0.33 ± 0.01	0.90 ± 0.17
36	0.76 ± 0.01	9.60 ± 0.56	0.43 ± 0.02	3.20 ± 0.30
55	0.77 ± 0.01	18.16 ± 0.65	0.51 ± 0.01	7.26 ± 0.30
89	0.80 ± 0.01	8.70 ± 0.40	0.52 ± 0.01	3.55 ± 0.13

show numerous islands. This thin ZnO layer increased recombination at the FTO/CH₃NH₃PbI₃ interface (Figure 4a) and caused poor performance of the device. PCEs reached up to 7% when a ZnO layer of approximately 55 nm was incorporated into the device. The smooth ZnO layer was completely covered on rough FTO surface (Figure 2c,f). PCE exhibited a distinctive decrease with further increase in the thickness of the ZnO layer to approximately 89 nm. The thick ZnO layer can cause large series resistance in devices and increase electron recombination.

To probe the influence of scanning conditions on photovoltaic performance, we conducted different scanning routines. Figure 4b and Table 2 show the current-density/voltage (*J*–*V*) characteristics and detailed photovoltaic parameters, respectively. Compared with the photovoltaic parameters under forward bias scan, the open-circuit voltage (*V*_{oc}), fill factor (FF), and PCE under inverse scan were higher than those under forward bias scan. Thus, the following *J*–*V* plot was performed under inverse bias scan. Figure 4c presents the PCEs of 10 individual ZnO/CH₃NH₃PbI₃/C PHJ-PSCs. Figure S1 shows the distributions of *V*_{oc}, short-circuit photocurrent (*J*_{sc}), and FF, whereas Figure 4d shows the *J*–*V* curves for the best-performing device. The values of *J*_{sc}, *V*_{oc}, FF, and PCE were 19.98 mA cm⁻², 810 mV, 0.54, and 8.73%, respectively. Figure 4e shows the incident-photon-to-current conversion efficiency (IPCE) for ZnO/CH₃NH₃PbI₃/C PHJ-PSCs. The IPCE value started at approximately 800 nm, which agrees with the band gap of CH₃NH₃PbI₃. The integrated current was 18.10 mA cm⁻², which agrees with the *J*–*V* results. Mott–Schottky plot (Figure 4f) was carried out to estimate the built-in potential in ZnO/CH₃NH₃PbI₃/C PHJ-PSCs by junction capacitance (eq 1).

$$\frac{1}{C^2} = \frac{2}{\epsilon \epsilon_0 q A^2 N} (V_{bi} - V) \quad (1)$$

where *C* is the measured capacitance, *A* is the active area, *V* is the applied bias, ϵ is the static permittivity, ϵ_0 is the permittivity of free space, *q* is the elementary charge, and *N* is the doping density of the donor. The intercept of the linear regime with the *x*-axis of the Mott–Schottky plot can be assigned to the built-in potential, ca. 0.91 V, suggesting that the photo-generated carriers can be separated by the presence of highly built-in field. In addition, the slope of Mott–Schottky plot in the linear regime was 9.2×10^{14} F⁻² V⁻¹ cm⁴, from which the net doping density in the CH₃NH₃PbI₃ was 0.51×10^{16} cm⁻³.

Flexible ZnO/CH₃NH₃PbI₃/C PHJ-PSCs were fabricated on ITO/PEN using the same preparation procedures as that on FTO/glass substrate. Figure S2 illustrates the photovoltaic performance of flexible ZnO/CH₃NH₃PbI₃/C PHJ-PSCs. For the best-performing flexible device (Figure 5a), the values for *J*_{sc}, *V*_{oc}, FF, and PCE were 13.38 mA cm⁻², 760 mV, 0.42, and 4.29%, respectively. Figure 5b shows the IPCE for flexible ZnO/CH₃NH₃PbI₃/C PHJ-PSCs. These flexible devices have potential for various applications despite their lower average PCE than that of the device prepared on rigid FTO-glass substrate.²⁴ They represent an important direction in modern electronics. Figure 5c shows a photograph that demonstrates the bending of the flexible ZnO/CH₃NH₃PbI₃/C PHJ-PSCs around one pen with a diameter of 1 cm. Bending tests (Figure 5d) indicated that the PCEs of flexible ZnO/CH₃NH₃PbI₃/C PHJ-PSCs could maintain 80% of their initial PCE after 1000 times of bending. The excellent performance of these light and flexible PHJ-PSCs is comparable to that of fiber-shaped PSC fabricated with HTM.¹⁶ In order to clarify the reason for the significantly lower performance of the PSC using flexible ITO/PEN substrate compared to FTO/glass substrate, the optical properties of substrates were tested. The transmittance of ITO/PEN substrate was lower than that of FTO/glass from 300 to 800 nm (Figure 5e). Figure 5f showed that absorption of ITO/PEN is stronger than that of FTO/glass, which agreed with the result of transmittance. Subtractive absorbance between the absorbance of FTO/glass and ITO/PEN is shown in Figure 5g. The wavelength of the biggest subtractive absorbance between

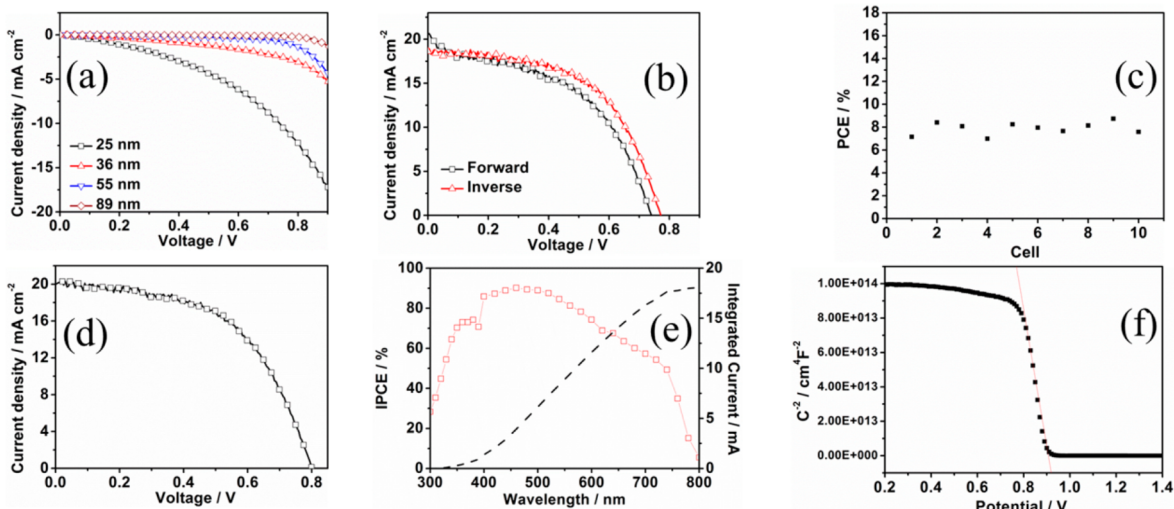


Figure 4. (a) J – V characteristics of $\text{ZnO}/\text{CH}_3\text{NH}_3\text{PbI}_3/\text{C}$ PHJ-PSCs prepared with varying thicknesses of ZnO in the dark. (b) Influence of scanning conditions on $\text{ZnO}/\text{CH}_3\text{NH}_3\text{PbI}_3/\text{C}$ PHJ-PSCs J – V : forward scan (from 0 to 1 V); inverse scan (from 1 to 0 V); scan rate: 84 mV/s. (c) PCE of 10 $\text{ZnO}/\text{CH}_3\text{NH}_3\text{PbI}_3/\text{C}$ PHJ-PSCs prepared on FTO/glass substrate and measured at a simulated AM1.5G solar irradiation of 100 mW cm^{-2} , 0.12 cm^2 mask. (d) J – V characteristics of the best performed $\text{ZnO}/\text{CH}_3\text{NH}_3\text{PbI}_3/\text{C}$ PHJ-PSCs prepared on FTO/glass substrate. (e) IPCE spectrum of $\text{ZnO}/\text{CH}_3\text{NH}_3\text{PbI}_3/\text{C}$ PHJ-PSCs. (f) Mott–Schottky plot of the $\text{ZnO}/\text{CH}_3\text{NH}_3\text{PbI}_3/\text{C}$ PHJ-PSC.

Table 2. Photovoltaic Parameters of $\text{ZnO}/\text{CH}_3\text{NH}_3\text{PbI}_3/\text{C}$ PHJ-PSCs under Different Test Conditions

test conditions	V_{oc}/V	$J_{sc}/\text{mA cm}^{-2}$	FF	PCE/%
forward	0.74 ± 0.02	20.68 ± 0.30	0.46 ± 0.02	7.05 ± 0.52
inverse	0.77 ± 0.02	18.56 ± 0.20	0.56 ± 0.02	8.07 ± 0.45

FTO/glass and ITO/PEN was at approximately 360 nm, which agreed with that of the biggest subtractive IPCE (Figure 5h) between the IPCE of FTO/glass and ITO/PEN. Thus, the low

transmittance of ITO/PEN compared to FTO/glass was one of the reasons for its lower performance.

Stability is a serious challenge in developing PSCs. Hence, the primary stability test of the flexible $\text{ZnO}/\text{CH}_3\text{NH}_3\text{PbI}_3/\text{C}$ PHJ-PSCs was conducted. The device without encapsulation was stored in air and at room temperature and measured in air under AM 1.5 G and 100 mW cm^{-2} solar irradiation. Supporting Information Figure S3 shows the good primary stability of the devices. The crystal structure of organometal trihalide perovskites are easily destroyed by H_2O . Our previous reported results²¹ demonstrated that the surface of our carbon

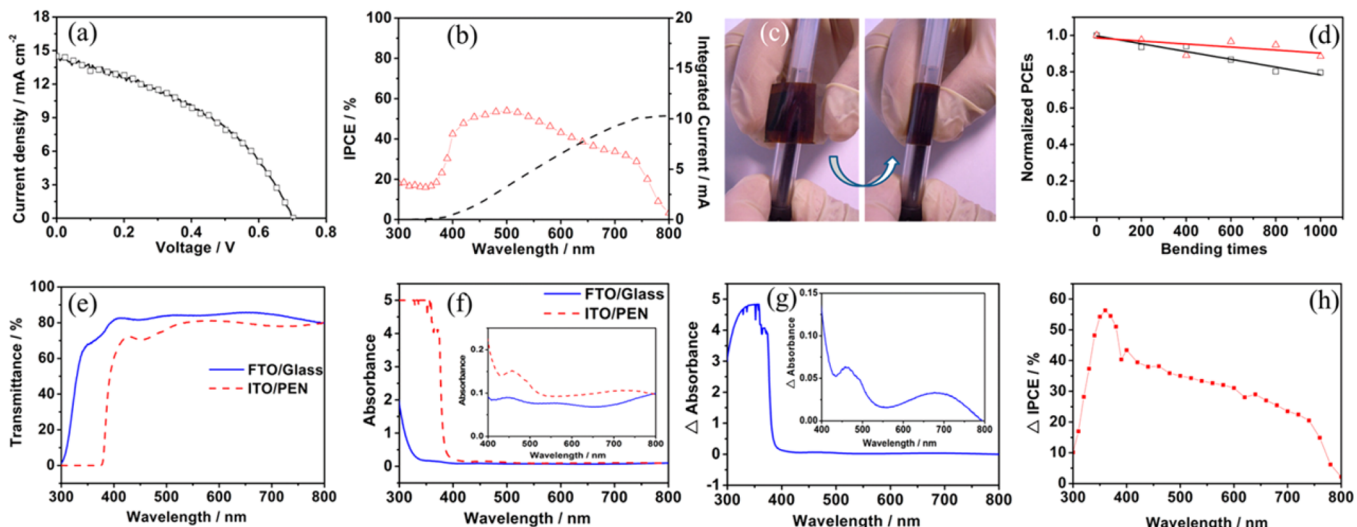


Figure 5. (a) J – V characteristics of the best performed flexible $\text{ZnO}/\text{CH}_3\text{NH}_3\text{PbI}_3/\text{C}$ PHJ-PSCs prepared on ITO/PEN substrate and measured at a simulated AM1.5G, 100 mW cm^{-2} solar irradiation. (b) IPCEs for flexible $\text{ZnO}/\text{CH}_3\text{NH}_3\text{PbI}_3/\text{C}$ PHJ-PSCs. (c) Photograph demonstrating the bending of the flexible $\text{ZnO}/\text{CH}_3\text{NH}_3\text{PbI}_3/\text{C}$ PHJ-PSCs around one pen with a diameter of 1 cm. (d) PCE variations after 1000 times bending of two randomly selected flexible $\text{ZnO}/\text{CH}_3\text{NH}_3\text{PbI}_3/\text{C}$ PHJ-PSCs around one pen with a diameter of 1 cm (red triangle or the black square in the figure represents one of the two randomly selected flexible devices). (e) Transmittance of FTO/glass and ITO/PEN. (f) UV–vis absorption spectrum of FTO/glass and ITO/PEN; inset: amplified plot from 400 to 800 nm. (g) Difference absorbance (Δ Absorbance) between the absorbance of FTO/glass and ITO/PEN; inset: amplified plot from 400 to 800 nm. (h) Difference IPCE (Δ IPCE) between the IPCE of $\text{ZnO}/\text{CH}_3\text{NH}_3\text{PbI}_3/\text{C}$ PHJ-PSCs based on FTO/glass substrate and that based on ITO/PEN substrate.

electrode was hydrophobic. This hydrophobic surface of the carbon electrode may benefit the stability of the cells without encapsulation when they are exposed to moisture. In addition, the free HTM with volatile additives may be another reason for the good stability for this very simple architecture of $\text{ZnO}/\text{CH}_3\text{NH}_3\text{PbI}_3/\text{C}$ PHJ-PSCs.

4. CONCLUSIONS

In summary, hole conductor-free, metal-electrode-free PHJ-PSCs were prepared on rigid and flexible substrate using thin film $\text{CH}_3\text{NH}_3\text{PbI}_3$ sandwiched between n-type ZnO as an electron-transport layer and carbon electrode as a hole-selective layer. The low-temperature processed $\text{ZnO}/\text{CH}_3\text{NH}_3\text{PbI}_3/\text{C}$ PHJ-PSCs achieved PCEs up to 8% on FTO/glass substrates and over 4% on flexible polymer substrates. The flexible device performed well after 1000 times of bending. These PSCs are low cost, have simple architecture and procedure, and benefit future large-scale production.

■ ASSOCIATED CONTENT

Supporting Information

V_{oc} , J_{sc} , and FF of 10 $\text{ZnO}/\text{CH}_3\text{NH}_3\text{PbI}_3/\text{C}$ PHJ-PSCs prepared on FTO/Glass substrate; photovoltaic parameters of seven individual flexible $\text{ZnO}/\text{CH}_3\text{NH}_3\text{PbI}_3/\text{C}$ PHJ-PSCs; primary stability of flexible $\text{ZnO}/\text{CH}_3\text{NH}_3\text{PbI}_3/\text{C}$ PHJ-PSCs. This material is available free of charge via the Internet at <http://pubs.acs.org>.

■ AUTHOR INFORMATION

Corresponding Authors

*E-mail: tinglima@dlut.edu.cn; phone: 86-411-84986237 (T.M.).

*E-mail: shiyantao@dlut.edu.cn; phone: 86-411-84986237 (Y.S.).

Notes

The authors declare no competing financial interest.

■ ACKNOWLEDGMENTS

This work was financially supported by National Natural Science Foundation of China (Grant No. 51273032 and 91333104), International Science & Technology Cooperation Program of China (Grant No. 2013DFA51000).

■ REFERENCES

- (1) Kojima, A.; Teshima, K.; Shirai, Y.; Miyasaka, T. Organometal Halide Perovskites as Visible-Light Sensitizers for Photovoltaic Cells. *J. Am. Chem. Soc.* **2009**, *131*, 6050–6051.
- (2) Im, J.-H.; Lee, C.-R.; Lee, J.-W.; Park, S.-W.; Park, N.-G. 6.5% Efficient Perovskite Quantum-Dot-Sensitized Solar Cell. *Nanoscale* **2011**, *3*, 4088–4093.
- (3) Kim, H.-S.; Lee, C.-R.; Im, J.-H.; Lee, K.-B.; Moehl, T.; Marchioro, A.; Moon, S.-J.; Humphry-Baker, R.; Yum, J.-H.; et al. Lead Iodide Perovskite Sensitized All-Solid-State Submicron Thin Film Mesoscopic Solar Cell with Efficiency Exceeding 9%. *Sci. Rep.* **2012**, *2*, 519.
- (4) Burschka, J.; Pellet, N.; Moon, S.-J.; Humphry-Baker, R.; Gao, P.; Nazeeruddin, M. K.; Graetzel, M. Sequential Deposition as a Route to High-Performance Perovskite-Sensitized Solar Cells. *Nature* **2013**, *499*, 316–320.
- (5) Lee, M. M.; Teuscher, J.; Miyasaka, T.; Murakami, T. N.; Snaith, H. J. Efficient Hybrid Solar Cells Based on Meso-Superstructured Organometal Halide Perovskites. *Science* **2012**, *338*, 643–647.
- (6) Ball, J. M.; Lee, M. M.; Hey, A.; Snaith, H. J. Low-Temperature Processed Meso-Superstructured to Thin-Film Perovskite Solar Cells. *Energy Environ. Sci.* **2013**, *6*, 1739–1743.
- (7) Leijtens, T.; Eperon, G. E.; Pathak, S.; Abate, A.; Lee, M. M.; Snaith, H. J. Overcoming Ultraviolet Light Instability of Sensitized TiO_2 with Meso-Superstructured Organometal Tri-Halide Perovskite Solar Cells. *Nat. Commun.* **2013**, *4*, 2885.
- (8) Wojciechowski, K.; Saliba, M.; Leijtens, T.; Abate, A.; Snaith, H. J. Sub-150 °C Processed Meso-Superstructured Perovskite Solar Cells with Enhanced Efficiency. *Energy Environ. Sci.* **2014**, *7*, 1142–1147.
- (9) Mingzhen, L.; Johnston, M. B.; Snaith, H. J. Efficient Planar Heterojunction Perovskite Solar Cells by Vapour Deposition. *Nature* **2013**, *501*, 395–398.
- (10) Zhou, H.; Chen, Q.; Li, G.; Luo, S.; Song, T.-B.; Duan, H.-S.; Hong, Z.; You, J.; Liu, Y.; Yang, Y. Photovoltaics. Interface Engineering of Highly Efficient Perovskite Solar Cells. *Science* **2014**, *345*, 542–546.
- (11) Ku, Z.; Rong, Y.; Xu, M.; Liu, T.; Han, H. Full Printable Processed Mesoscopic $\text{CH}_3\text{NH}_3\text{PbI}_3/\text{TiO}_2$ Heterojunction Solar Cells with Carbon Counter Electrode. *Sci. Rep.* **2013**, *3*, 3132.
- (12) Mei, A.; Li, X.; Liu, L.; Ku, Z.; Liu, T.; Rong, Y.; Xu, M.; Hu, M.; Chen, J.; Yang, Y.; et al. A Hole-Conductor-Free, Fully Printable Mesoscopic Perovskite Solar Cell with High Stability. *Science* **2014**, *345*, 295–298.
- (13) Li, Z.; Kulkarni, S. A.; Boix, P. P.; Shi, E.; Cao, A.; Fu, K.; Batabyal, S. K.; Zhang, J.; Xiong, Q.; Wong, L. H.; et al. Laminated Carbon Nanotube Networks for Metal Electrode-Free Efficient Perovskite Solar Cells. *ACS Nano* **2014**, *8*, 6797–804.
- (14) Liu, D.; Kelly, T. L. Perovskite Solar Cells with a Planar Heterojunction Structure Prepared Using Room-Temperature Solution Processing Techniques. *Nat. Photonics* **2014**, *8*, 133–138.
- (15) Docampo, P.; Ball, J. M.; Darwich, M.; Eperon, G. E.; Snaith, H. J. Efficient Organometal Trihalide Perovskite Planar-Heterojunction Solar Cells on Flexible Polymer Substrates. *Nat. Commun.* **2013**, *4*, 2761.
- (16) Qiu, L.; Deng, J.; Lu, X.; Yang, Z.; Peng, H. Integrating Perovskite Solar Cell into a Flexible Fiber. *Angew. Chem., Int. Ed.* **2014**, *S3*, 10425–10428.
- (17) You, J.; Hong, Z.; Yang, Y.; Chen, Q.; Cai, M.; Song, T.-B.; Chen, C.-C.; Lu, S.; Liu, Y.; Zhou, H. Low-Temperature Solution-Processed Perovskite Solar Cells with High Efficiency and Flexibility. *ACS Nano* **2014**, *8*, 1674–1680.
- (18) Chiang, Y.-F.; Jeng, J.-Y.; Lee, M.-H.; Peng, S.-R.; Chen, P.; Guo, T.-F.; Wen, T.-C.; Hsu, Y.-J.; Hsu, C.-M. High Voltage and Efficient Bilayer Heterojunction Solar Cells Based on an Organic–Inorganic Hybrid Perovskite Absorber with a Low-Cost Flexible Substrate. *Phys. Chem. Chem. Phys.* **2014**, *16*, 6033–6040.
- (19) Kumar, M. H.; Yantara, N.; Dharani, S.; Graetzel, M.; Mhaisalkar, S.; Boix, P. P.; Mathews, N. Flexible, Low-Temperature, Solution Processed ZnO -based Perovskite Solid State Solar Cells. *Chem. Commun.* **2013**, *49*, 11089–11091.
- (20) Roldan-Carmona, C.; Malinkiewicz, O.; Soriano, A.; Minguez Espallargas, G.; Garcia, A.; Reinecke, P.; Kroyer, T.; Dar, M. I.; Nazeeruddin, M. K.; Bolink, H. J. Flexible High Efficiency Perovskite Solar Cells. *Energy Environ. Sci.* **2014**, *7*, 994–997.
- (21) Zhou, H.; Shi, Y.; Dong, Q.; Zhang, H.; Xing, Y.; Wang, K.; Du, Y.; Ma, T. Hole-Conductor-Free, Metal-Electrode-Free $\text{TiO}_2/\text{CH}_3\text{NH}_3\text{PbI}_3$ Heterojunction Solar Cells Based on a Low-Temperature Carbon Electrode. *J. Phys. Chem. Lett.* **2014**, *5*, 3241–3246.
- (22) Kavan, L.; Prochazka, J.; Spitzer, T. M.; Kalbac, M.; Zukalova, M. T.; Drezen, T.; Gratzel, M. Li Insertion into $\text{Li}_4\text{Ti}_5\text{O}_{12}$ p(Spinel) - Charge Capability vs. Particle Size in Thin-Film Electrodes. *J. Electrochem. Soc.* **2003**, *150*, A1000–A1007.
- (23) Baikie, T.; Fang, Y.; Kadro, J. M.; Schreyer, M.; Wei, F.; Mhaisalkar, S. G.; Graetzel, M.; White, T. J. Synthesis and Crystal Chemistry of the Hybrid Perovskite $(\text{CH}_3\text{NH}_3)\text{PbI}_3$ for Solid-State Sensitised Solar Cell Applications. *J. Mater. Chem. A* **2013**, *1*, 5628–5641.

- (24) Li, L.; Wu, Z.; Yuan, S.; Zhang, X.-B. Advances and Challenges for Flexible Energy Storage and Conversion Devices and Systems. *Energy Environ. Sci.* **2014**, *7*, 2101–2122.